are not incompatible and may operate together to allow the rapid switch between dike and sill intrusions.

One of the goals of sub-ridge asthenopheric models is to explain how melt is focused at the ridge[10]. The sheet-intrusion net described here may be part of the explanation, with sills and ridge-perpendicular dikes capturing flow from ridge-parallel dikes, and moving it to the ridge axis. One could propose, to explain the observed system, a simple elastic model in which a local switch between the principal stresses would be related only to dike intrusion itself. We believe (on the basis of the field arguments) that it is better explained by including in the model the effect on the stress field of plastic flow in the upper mantle. Such a 'breathing ridge' model implies that at the onset of the melt surge, even at Moho depth beneath the ridge axis, the regional lithospheric stress field can temporarily predominate over the more local asthenospheric stress field that is related to the diapir uprise. This model explains how, during a single magmatic event, lithospheric and asthenospheric control may be exerted successively, allowing dikes and sills to be opened almost simultaneously. □

Received 24 June; accepted 25 October 1993.

1. Nicolas, A. *Structures in Ophiolites and Dynamics of Oceanic Lithosphere* (Kluwer, Dordrecht, 1989).
2. Nicolas, A., Boudier, F. & Ildefonse, B. in *Magmatic Systems* (ed. Ryan, M. P.) (Academic, Orlando, in the press).
3. Kelemen, P. B., Dick, H. J. B. & Quick, J. E. *Nature* **358,** 635–641 (1992).
4. Nehlig, P. & Juteau, T. *Tectonophysics* **151,** 199–221 (1988).
5. Nicolas, A. & Jackson, M. *J. Petrology* **23,** 568–582 (1982).
6. Sleep, N. H. *J. geophys. Res.* **93,** 10255–10272 (1988).
7. Foulger, G. R. *et al. Nature* **358,** 488–490(1992).
8. Rubin, A. M. *Bull. Volcan.* **52,** 302–319 (1990).
9. Rabinowicz, M., Ceuleneer, G. & Nicolas, A. *J. geophys. Res.* **92,** 3475–3486 (1987).
10. Su, W. & Buck, R. *J. geophys. Res.* **98,** 12191–12205 (1993).
11. Scott, D. R. & Stevenson, D. J. *J. geophys. Res.* **94,** 2973–2988 (1989).
12. Nicolas, A., Freydier, C., Godard, M. & Vauchez, A. *Geology* **21,** 53–56 (1993).

ACKNOWLEDGMENTS. We thank N. Sleep and A. Rubin for reviews of this manuscript, and A. Vauchez and B. Celerier for discussions and comments. We acknowledge contributions to field measurements by E. Gnos, G. Ceuleneer, I. Reuber, M. Misseri, K. Benn and C. MacLeod. The term 'breathing ridge' was suggested by J. Pallister.

Seismic anisotropy in the mantle beneath an oceanic spreading centre

Donna K. Blackman*, John A. Orcutt*, Donald W. Forsyth† & J-Michael Kendall*‡

* Institute of Geophysics and Planetary Physics, Scripps Institution of Oceanography, La Jolla, California 92093-0225, USA
† Department of Geological Sciences, Brown University, Providence, Rhode Island 02912, USA

BENEATH an active mid-ocean ridge, the mantle upwells in response to the divergence of the newly formed plates, leading to high temperatures and pressure-release melting below the ridge axis. The width of the upwelling region and the amount of melting depend on mantle rheology[1–5], but all models predict a maximum decrease in seismic velocity at the ridge axis. It has also been suggested, however, that the alignment of anisotropic minerals by shear in the upwelling mantle will increase seismic velocity for rays travelling subvertically through the upwelling zone[6,7]. Here we report the observation of a consistent pattern of anomalously early P-wave arrival times at an array of ocean-bottom seismographs deployed across the axis of the southern Mid-Atlantic Ridge: P-waves from distant earthquakes arrive earlier at stations near the axis than at those further away. Our results are consistent with a model of anisotropy in which the degree of mineral alignment is greatest directly beneath the ridge axis, and significant anisotropy extends tens of kilometres from the axis.

Three earthquakes of magnitude greater than 6 were recorded during a 4-week deployment of ocean-bottom seismographs (OBSs) at the Mid-Atlantic Ridge (MAR; 34° S) in Spring 1990. The OBS array consisted of six instruments, three spaced ~25 km apart of the western flank of the ridge and three similarly spaced on the eastern ridge flank (Fig. 1). Relative plate velocities average 35 km Myr^{-1} along this section of the MAR and the morphology is characteristic of a slow-spreading centre[8–10].

The teleseismic data comprise 19 long-period recordings of P-phases from 3 sources (Table 1). Cross-correlation of the individual phases was used to determine the relative travel times to different instruments in the array. In every case, the near-axis OBSs record the P-waves 0.4–1.5 s earlier than the off-axis stations (Table 1 and Fig. 2). Within the data uncertainty of 0.25 s, an increase in relative delay with distance from the axis is evident: 0.6 s delay ~50 km off-axis; 1.2 s ~75 km off-axis.

The main contribution to the travel-time anomalies across the OBS array comes from the uppermost mantle. Near-source and along-path effects are eliminated as the paths of the rays are essentially identical at teleseismic distances and we use relative travel times. Variations in mantle temperature or the thickness of the crust could affect travel times, but we estimate the size of

TABLE 1 Relative travel time of P-phases

Earthquake P-phase*	ΔFRD† (s)	Xcorr‡ (s)	Delay§ (s)
0405 PKP			
OPS	+0.42	+0.50	0.08
FRD	0	0	0
KRN	−0.12	+0.66	0.78
JDY	−0.36	+0.75	1.11
0405 PP			
FRD	0	0	0
KRN	−0.54	+0.06	0.60
JDY	−1.32	+0.06	1.38
0418 PKP			
JAN	+1.08	+0.13	0.95
FRD	0	0	0
KRN	−0.30	+0.13	0.43
JDY	−0.66	+0.16	0.82
0418 PP			
JAN	+3.72	+4.12	0.40
FRD	0	0	0
KRN	−0.96	−0.25	0.71
JDY	−2.10	−0.62	1.48
0403 P			
JAN	−3.42	−2.84	0.58
FRD	0	0	0
KRN	+0.90	+2.34	1.44
JDY	+1.68	+2.59	0.91

Relative travel times of P-phases determined from differential pressure gauge records at seismometers JAN, OPS, FRD, KRN and JDY. (During earthquake 0405, JAN was in the process of writing to tape so did not record the event. OPS had inconsistencies in sampling rate so only the unfiltered data for the largest event (earthquake 0405) was used from this instrument.)

* P-phase and earthquake for which the listed instruments have data.

† Travel time relative to ocean-bottom seismograph (OBS) FRD as predicted by reference Earth model PREM.

‡ Observed travel times relative to FRD as determined from cross-correlation of waveforms.

§ Travel-time anomaly relative to PREM; arrivals are earliest at the near-axis stations FRD and OPS.

‡ Present address: Department of Physics, University of Toronto, Toronto, Ontario M5S 1A7, Canada.

these contributions to be similar in magnitude to the uncertainties in our analysis. Gravity anomalies inferred to reflect crustal thickness variations beneath our OBS array[11] suggest corresponding travel-time anomalies of <0.25 s. Advection of hot mantle from depth results in higher temperatures, therefore slower seismic velocities, in the upwelling region compared to the surrounding mantle[12,13]. Converting oceanic PP-P residuals[14] to one-way vertical travel times versus plate age (-0.07 s $Myr^{-1/2}$) gives an axial thermal delay of only 0.15 s relative to a distance off-axis equal to the half-width of our array.

More important than the solid-state effect of high subaxial temperatures is the partial melting that occurs. The resulting basaltic liquid has significantly lower seismic velocities than ambient mantle, but its detectability depends critically on how the melt is distributed in the host rock[15]. The presence of as little as 1% melt fraction distributed in a triangular region of 120-km wide base at 60 km depth will delay P-waves by ~0.1 s (refs 16, 17). The fact that we do not find slow near-axis arrivals in our data suggests that either the amount of melt present at this location is small or that the melt zone extends <25 km off-axis. The presence of a narrow melt zone may be suggested by a previous measurement of teleseismic P-wave delay at the northern MAR, where arrivals at an instrument within the axial median valley were 0.5-s later than arrivals at the rift walls[18].

Shear stresses that develop during viscous flow of the mantle are predicted to result in seismic anisotropy in the deformed peridotite. Field studies in ophiolites indicate that the *a*-axis of olivine crystals aligns towards the direction of the shear plane during deformation of the mantle[19,20]. Compressional seismic energy travels along the *a*-axis of olivine 22% faster than it does along the *b*-axis[20]. As the dominant shear plane beneath a (two-dimensional) spreading centre is vertical, a detectable travel-time anomaly could accrue as P-waves travel through the upwelling zone. It is not yet clear exactly how factors that could influence subaxial anisotropy interact (for example, mantle stress field, the degree to which olivine crystals within an aggregate align, the dominant direction of that alignment and the change in elastic constants) but results so far indicate that it is a potentially significant contributor to the relative travel times across a spreading centre[17,20–22].

Seismic modelling shows that the observed near-axis travel-time advance can be reasonably attributed to anisotropy in the upwelling region for a plausible spreading-centre velocity structure (Fig. 2). The model shown is one in a series for which the travel-time contributions of melt, lithospheric anisotropy, and upwelling mantle anisotropy were evaluated[17]. Seismic rays are traced through the model with a computer programme that incorporates the effects of three-dimensional heterogeneous, anisotropic structure[23]. Rays are traced initially through a spherically symmetric global model, PREM, for ranges comparable to the observed earthquakes (Fig. 1, top). At a depth of 80 km, rays spaced a few kilometres apart enter the bottom of the prescribed ridge velocity structure. The model that best fits the southern MAR data contains a lithosphere that thickens off-axis at a rate appropriate for the spreading rate of 18 mm yr^{-1} and has 7% anisotropy with the fast-axis horizontal. There is no melt present and the only temperature condition is that embodied in the definition of lithospheric thickness which increases with the square root of plate age. The anisotropy due to upwelling is prescribed in a region centred on the axis that has a maximum value out to 30 km, then is cosine-tapered to <1% (essentially isotropic) at 60 km off-axis; 15% anisotropy in the upwelling region is required to fit the data.

There is some trade-off between the amount of anisotropy determined for the upwelling region, its depth, and the anisotropy in the lithosphere, but we cannot fit the data without significant vertical anisotropy near the axis. The choice of 7% horizontal anisotropy in the lithosphere is based on several previous studies (for example, refs 24–27) that determined the average anisotropy for large areas. It is possible that these average values contain locally greater degrees of lithospheric anisotropy. We could reduce the required amount of upwelling anisotropy by a few per cent if we increased the lithospheric anisotropy, but the smooth nature of the increase in plate thickness off-axis precludes a major reduction in upwelling anisotropy because the data indicate that the travel-time anomaly is relatively narrow. If we doubled the depth of the anisotropic upwelling we could reduce the required degree of anisotropy to a value similar to that in the lithosphere. The depth to which spreading-centre dynamics control the mantle stress field is not well constrained; our choice of 80 km as the base of the model reflects the depth at which significant across-axis variability may begin to develop due to the onset of melting.

The 60-km half-width of the anisotropic upwelling region is constrained to within <10 km for the simple geometry assumed. On a global scale, the width of this inferred region of high anisotropy is quite small. It would be difficult to resolve this feature using land seismic stations because the bounce-point coverage does not typically span spreading axes. This, combined with the use of S-waves which show little anomalous behaviour in response to vertically aligned crystal anisotropy for near-vertical raypaths[17], may be why previous SS-S studies did not detect an axial anomaly[27,28]. Our inferred degree of upwelling anisotropy seems high but this value is not unprecedented. Wide-angle reflection data off Norway can be explained by 15% anisotropy in the upper mantle[29] although in this case the anisotropy is attributed to shearing associated with a dipping master fault

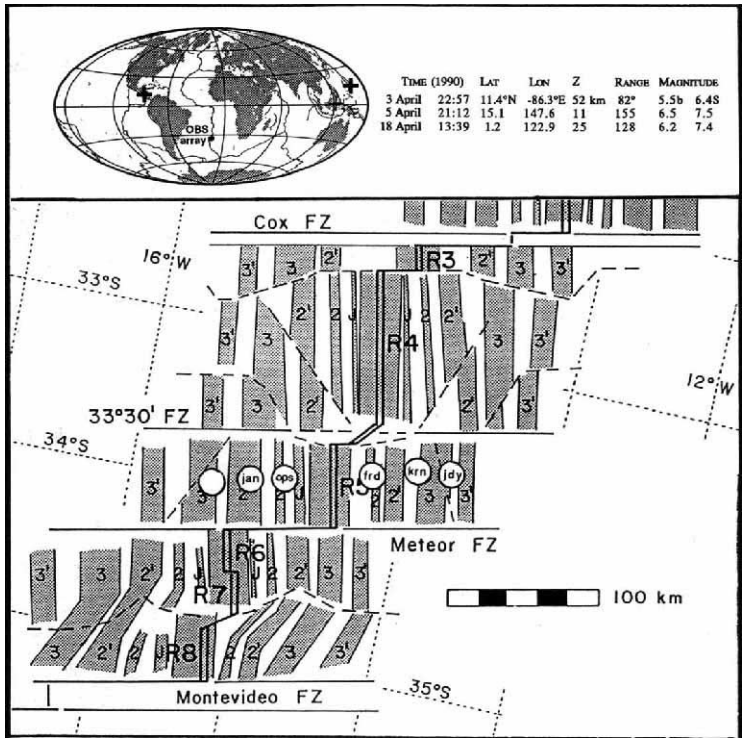

FIG. 1 Location of seismometer array. Top, map showing the position of the array along the mid-ocean ridge and also the locations (+) of the 3 earthquakes used in our analysis. Bottom, diagram showing the tectonic setting of the experiment within a series of ridge segments R (double heavy lines) and fracture zones FZ (light lines). Magnetic anomalies are identified on shaded stripes. Specific instrument names are circled to indicate their position relative to the spreading axis (the instrument on the extreme left is not discussed in this paper because the differential pressure-gauge channel was unreadable).

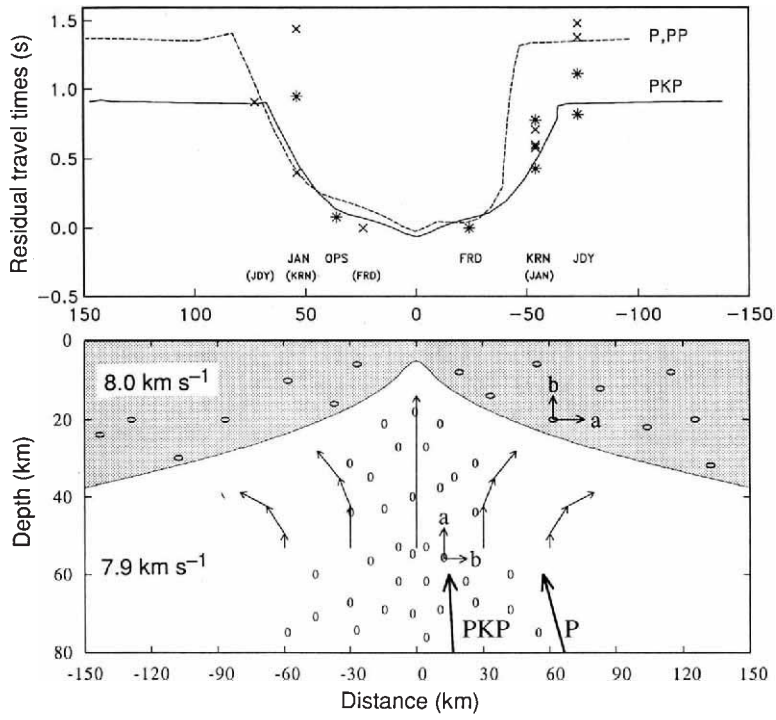

FIG. 2 Comparison of observed and modelled P-wave travel times at a slow-spreading centre. Bottom, sketch illustrating mantle flow (light arrows), off-axis thickening of plates (shaded), and anisotropy in upwelling region (ellipses). The long axis of an ellipse indicates the orientation of the *a*-axis of olivine, which is the fast direction for P-waves; the *b*-axis lies in the plane of the figure and the *c*-axis is perpendicular to this plane. The density of ellipses illustrates the degree of anisotropy which reaches a maximum of 15% in the subaxial region and tapers to <1% between 30 and 60 km off-axis. Anisotropy frozen into the plate (7%) is horizontal due to rotation of stresses near the surface. Angle of P-waves at the base of the model is indicated by heavy arrows. Top, residual travel times calculated for densely-spaced rays are plotted for PKP- (solid line) and PP-, P- (broken line) arrivals. PKP phase data shown by an asterisk, PP and P phases by a cross. Model delays are for phases traversing upwards from right to left so, for consistency, the data from earthquake 0403 are flipped with respect to the axis; the corresponding OBS names are shown in parentheses. The misfit between the 0403 P-wave at KRN and the model may be due to delays associated with travel through the ridge-offset region between R4 and R5 (Fig. 1).

that formed during regional extension. Recent modelling of the response of polycrystalline mantle rock to shear flow[30] suggests that the high degree of olivine alignment that develops during convective upwelling may be diffused as the flow turns to follow the direction of plate spreading. Thus, the estimated 7–8% of lithospheric anisotropy may not reflect the maximum possible mantle values.

Our data are few in number and site-specific, so we do not wish to interpret the results as a general indication that crystal alignment due to shear flow overwhelms other signals at all mid-ocean ridges. At slow-spreading systems, enhancement of the vertical flow rates (and presumably a corresponding increase in degree of anisotropy) in a narrow region beneath the axis can be caused by buoyancy-driven upwelling[4,5]. Conversely, at a fast-spreading centre, the high upwelling rates tend to overwhelm buoyancy-driven flow, so we might expect smaller relative travel-time anomalies due to shear-induced anisotropy than are observed at the southern MAR.

At present we are not able to use the shape of the observed travel-time anomaly to tightly constrain the width of the upwelling zone, because of uncertainties in the relationship between mantle shear, aligned melt and the development of seismic anisotropy. If the qualitative model of seismic anisotropy oriented in the direction of flow is correct, then the 60–70 km wide early-arrival region may reflect enhanced upwelling due to the presence of high melt fractions (for example, ref. 1). On the other hand, initial quantitative models of subaxial mantle structure and seismic anisotropy suggest that deformation can result in fast-axis orientations that are inclined to the flow direction by 30°–40° (refs 21, 22, 30) and that the presence of aligned melt films or melt-filled cracks can produce anisotropic behaviour as well[17]. A combination of additional teleseismic observations at mid-ocean ridges and theoretical modelling of the possible waveform effects of anisotropy distributions produced by different mechanisms are required in order to fully interpret the travel-time signal at the sea floor. The most diagnostic experiments will record both P- and S-phases on OBS arrays that span the axis with receivers both in the axial region and extending well beyond the half-width predicted for the upwelling zone by passive flow models at the appropriate spreading rate. □

Received 9 August; accepted 22 October 1993.

1. Buck, W. R. & Su, W. *Geophys. Res. Lett.* **16,** 641–644 (1989).
2. Sotin, C. & Parmentier, E. M. *Geophys. Res. Lett.* **16,** 835–838 (1989).
3. Scott, D. R. & Stevenson, D. J. *J. geophys. Res.* **94,** 2973–2988 (1989).
4. Turcotte, D. L. & Phipps Morgan, J. in *Mantle Flow and Melt Generation at Mid-Ocean Ridges* (eds Phipps Morgan, J., Blackman, D. K. & Sinton, J. M.) 155–182 (Am. geophys. Un., Washington DC, 1992).
5. Scott, D. R. in *Mantle Flow and Melt Generation at Mid-Ocean Ridges* (eds Phipps Morgan, J., Blackman, D. K. & Sinton, J. M.) 327–352 (Am. geophys. Un., Washington DC, 1992).
6. Anderson, D. L. *Theory of the Earth* (Blackwell Scientific, Boston, 1989).
7. Forsyth, D. W. in *Mantle Flow and Melt Generation at Mid-Ocean Ridges* (eds Phipps Morgan, J., Blackman, D. K. & Sinton, J. M.) 1–66 (Am. geophys. Un., Washington DC, 1992).
8. Macdonald, K. C. *A. Rev. Earth planet. Sci.* **10,** 155–190 (1982).
9. Kuo, B-Y., Forsyth, D. W. *Mar. Geophys. Res.* **10,** 205–232 (1988).
10. Carbotte, S., Welch, S. M. & Macdonald, K. C. *Mar. Geophys. Res.* **13,** 51–80 (1991).
11. Neumann, G. A. & Forsyth, D. W. *J. geophys. Res.* **98,** 17891–17910 (1993).
12. Sleep, N. *J. geophys. Res.* **74,** 542–549 (1969).
13. Phipps Morgan, J. & Forsyth, D. W. *J. geophys. Res.* **93,** 2955–2966 (1988).
14. Woodward, R. L. & Masters, G. *J. geophys. Res.* **96,** 6351–6377 (1991).
15. Schmeling, H. *Phys. Earth planet. Inter.* **41,** 34–57 (1985).
16. Faul, U., Toomey, D. R. & Humphreys, E. *Seismic Imaging of the East Pacific Rise Upper Mantle* (RIDGE Office Report, Woods Hole, 1992).
17. Kendall, J-M. *Geophys. Res. Lett.* (in the press).
18. Rowlett, H. & Forsyth, D. W. *Geophys. Res. Lett.* **6,** 273–276 (1979).
19. Nicolas, A., Boudier, F. & Boullier, A. M. *Am. J. Sci.* **273,** 853–876 (1973).
20. Christensen, N. I. *Geophys. J. R. Astr. Soc.* **76,** 89–111 (1984).
21. Ribe, N. M. *J. geophys. Res.* **94,** 4123–4223 (1989).
22. Wenk, H-R., Bennett, K., Canova, G. R. & Molinari, A. *J. geophys. Res.* **96,** 8337–8349 (1991).
23. Guest, W. S. & Kendall, J-M. *Can. J. Explor. Geophys.* (in the press).
24. Raitt, R. W., Shor, G. G., Francis, T. J. G. & Morris, G. B. *J. geophys. Res.* **74,** 3095–3109 (1969).
25. Forsyth, D. W. *Geophys. J. R. astr. Soc.* **43,** 103–162 (1975).
26. Nishimura, C. E. & Forsyth, D. W. *Geophys. J. Int.* **94,** 479–501 (1988).
27. Kuo, B-Y., Forsyth, D. W. & Wysession, M. *J. geophys. Res.* **92,** 6421–6436 (1987).
28. Sheehan, A. F. & Solomon, S. C. *J. geophys. Res.* **96,** 19981–20009 (1991).
29. Mjelde, R. & Sellevoll, M. A. *Tectonophysics* **222,** 21–32 (1993).
30. Chastel, T. B., Dawson, P. R., Wenk, H-R. & Bennett, K. *J. geophys. Res.* (in the press).